Accepted Manuscript

Design, synthesis and biological evaluation of 1-hydroxy-2-phenyl-4-pyridyl-1*H*-imidazole derivatives as xanthine oxidase inhibitors

Tingjian Zhang, Yunying Lv, Yu Lei, Dan Liu, Yao Feng, Jiaxing Zhao, Shaolei Chen, Fanhao Meng, Shaojie Wang

PII: S0223-5234(18)30073-4

DOI: 10.1016/j.ejmech.2018.01.060

Reference: EJMECH 10137

To appear in: *European Journal of Medicinal Chemistry*

Received Date: 9 November 2017

Revised Date: 5 January 2018

Accepted Date: 18 January 2018

Please cite this article as: T. Zhang, Y. Lv, Y. Lei, D. Liu, Y. Feng, J. Zhao, S. Chen, F. Meng, S. Wang, Design, synthesis and biological evaluation of 1-hydroxy-2-phenyl-4-pyridyl-1*H*-imidazole derivatives as xanthine oxidase inhibitors, *European Journal of Medicinal Chemistry* (2018), doi: 10.1016/j.ejmech.2018.01.060.

Design, synthesis and biological evaluation of 1-hydroxy-2-phenyl-4-pyridyl-1*H*-imidazole derivatives as xanthine oxidase inhibitors

Tingjian Zhang[a, b, 1], Yunying Lv[a, 1], Yu Lei[a], Dan Liu[a], Yao Feng[a], Jiaxing Zhao[a], Shaolei Chen[a], Fanhao Meng[b, *], Shaojie Wang[a, *]

[a]*Key Laboratory of Structure-Based Drugs Design & Discovery of Ministry of Education, School of Pharmaceutical Engineering, Shenyang Pharmaceutical University, 103 Culture Road, Shenhe District, Shenyang 110016, China*

[b]*School of Pharmacy, China Medical University, 77 Puhe Road, North New Area, Shenyang 110122, China*

*Corresponding authors.

Tel/Fax: +86-24-43520230, E-mail: sjwang_99@163.com (S. J. Wang);

Tel.: +86-24-31939448, E-mail: fhmeng@cmu.edu.cn (F. H. Meng).

[1] These two authors contributed equally to this work.

Abstract

In our previous study, we reported a series of 1-hydroxy-2-phenyl-1*H*-imidazole-5-carboxylic acid derivatives that presented excellent in vitro xanthine oxidase inhibitory potency. As a continuation study, a series of 1-hydroxy-2-phenyl-1*H*-imidazole derivatives containing a pyridine moiety (**4a-g** and **5a-g**) at the 4-position was designed and synthesized. Evaluation of in vitro xanthine oxidase inhibition demonstrated that the **4a-g** series was more potent than the **5a-g** series. Compound **4f** was the most promising derivative in the series with an IC_{50} value of 0.64 μM. A Lineweaver-Burk plot revealed that compound **4f** acted as a mixed-type xanthine oxidase inhibitor. An *iso*-pentyloxy group at the 4′-position improved the inhibitory potency. More interestingly, structure-activity relationship analysis indicated that the pyridine *para*-N atom played a crucial role in the inhibition. Molecular modeling provided a reasonable explanation for the structure-activity relationships observed in this study. In addition, a three dimensional quantitative structure-activity relationships model which possessed reasonable statistics (q^2 = 0.885 and r^2 = 0.993) was conducted to further understand the structural basis of these compounds as xanthine oxidase inhibitors. These compounds, especially compound **4f**, have good potential for further investigations.

Keywords: 1-Hydroxy-2-phenyl-4-pyridyl-1*H*-imidazole; Synthesis; Xanthine oxidase inhibitor; Hyperuricemia

1. Introduction

Xanthine oxidase (XO) is a key enzyme in purine metabolism that catalyzes the hydroxylation of both hypoxanthine and xanthine in the last two steps of urate biosynthesis in humans [1, 2]. In parallel with the hydroxylation, reactive oxygen species (ROS) are produced [3]. Therefore, inhibition of XO not only effectively reduces the production of uric acid for the treatment of hyperuricemia and gout, but also benefits the pathological conditions caused by the XO-derived ROS such as oxidative damage, post-ischemic reperfusion injury, diabetes and chronic heart failure [4-6]. Allopurinol (**Fig. 1**), a prototype XO inhibitor and a hypoxanthine isomer, has been widely prescribed in the treatment of hyperuricemia and gout for several decades. However, in some cases, severe life-threatening side effects, including fulminant hepatitis, renal failure, and Stevens–Johnson syndrome, due to the similar backbone with purine have been reported [7]. Under these limitations, there is an immense need for non-purine XO inhibitors to be developed with potent XO inhibitory activity but fewer side effects.

In recent years, a great amount of non-purine XO inhibitors have been reported. Febuxostat [8] (**Fig. 1**) is a novel non-purine XO inhibitor that showed a more potent and longer-lasting urate-lowering effect than allopurinol and was approved in USA in 2009 for the treatment of gout. Topiroxostat (also known as FYX-051, **Fig. 1**) is another type of XO inhibitor approved in Japan in 2013. It not only interacts with amino acid residues of the active pocket but also forms a covalent linkage to molybdenum via oxygen in the hydroxylation reaction process [9]. In addition, other XO inhibitors have been reported in the literature including Y-700 [10], selenazoles [11], 1,2,3-triazoles [12], 2-(indol-5-yl)thiazoles [13], phenyl-1,2,4-triazoles [14], 4-(pyridin-4-yl)-1,2,3-triazoles [15], isonicotinamides [16], isocytosines [17-20], isoxazoles [21], *N*-(1,3-diaryl-3-oxo-propyl)amides [22], *N*-acetyl pyrazolines [23], chalcones [24], fraxamoside [25],

pyrano[3,2-d]pyrimidines [26], benzaldehydes [27], 2-arylbenzo[b]furans [28] and 2-benzamido-4-methylthiazole-5-carboxylic acids [29].

In our previous report, we employed an imidazole moiety, as an isostere, to replace the thiazole of Febuxostat and designed a series of 1-hydroxy-2-phenyl-1*H*-imidazole-5-carboxylic acid derivatives [30]. These compounds displayed excellent in vitro potency, especially, compounds **1-3** (**Fig. 1**) showed higher activity than the positive control Febuxostat. Structure activity relationship (SAR) analysis and molecular modeling studies indicated that the 1-hydroxy could form an extra H-bond with Thr1010 and contribute to the inhibitory potency [30]. The results inspired us to further explore novel XO inhibitors based on the 1-hydroxyimidazole moiety. With compounds **1-3** and Topiroxostat as leading compounds, in this study, we retained the 1-hydroxy-2-phenylimidazole fragment of **1-3** and hybridized the pyridine moiety of Topiroxostat (**Fig. 2**) to obtain a series of 1-hydroxy-2-phenyl-4-pyridyl-1*H*-imidazole derivatives (**4a-g** and **5a-g**) by the molecular hybrid method, hoping that, on one hand, the 1-hydroxy-2-phenylimidazole fragment could maintain its interactions with XO, and on the other hand, the pyridine moiety could pick up an interaction mode with XO similar to that of Topiroxostat. In addition, molecular modeling studies, three dimensional quantitative structure-activity relationships (3D-QSAR) and steady-state kinetic analysis were also performed to investigate the inhibition behaviors of these compounds.

2. Results and discussion

2.1. Chemistry

The synthesis of 2-(4-alkoxy-3-cyanophenyl)-1-hydroxy-4-(pyridin-4-yl)-1*H*-imidazoles (**4a-f**) and

2-(4-alkoxy-3-cyanophenyl)-1-hydroxy-4-(pyridin-3-yl)-1*H*-imidazoles (**5a-f**) was performed as outlined in **Scheme l**. Commercially available 4-hydroxybenzaldehyde was brominated with bromine catalyzed by iodine in dichloromethane to obtain 3-bromo-4-hydroxybenzaldehyde (**6**), which was alkylated with benzyl bromide in DMF in the presence of anhydrous potassium carbonate to provide 3-bromo-4-benzoxybenzaldehyde (**7**). Compound **7** was cyanided with cuprous cyanide followed by the removal of the benzyl protecting group under hydrogen atmosphere catalyzed by Pd/C in THF to yield the key intermediate **9**. Compound **9** was alkylated with various alkyl chlorides or alkyl bromides to obtain 4-alkoxy-3-cyanobenzaldehydes (**10a-f**).

Commercially available 1-(pyridin-4-yl)ethan-1-one and 1-(pyridin-3-yl)ethan-1-one were treated with *tert*-butyl nitrite in a sodium ethoxide solution to provide 2-oxo-2-(pyridin-4-yl)acetaldehyde oxime (**11**) and 2-oxo-2-(pyridin-3-yl)acetaldehyde oxime (**12**), respectively. Cyclization of **11** and **12** with intermediates **10a-f** led to 2-(4-alkoxy-3-cyanophenyl)-1-hydroxy-4-(pyridin-4-yl)-1*H*-imidazoles (**4a-f**) and 2-(4-alkoxy-3-cyanophenyl)-1-hydroxy-4-(pyridin-3-yl)-1*H*-imidazoles (**5a-f**), respectively. By the same procedure, compounds **11** and **12** cyclized with commercially available 3-cyanobenzaldehyde provided 2-(3-cyanophenyl)-1-hydroxy-4-(pyridine-4-yl)-1*H*-imidazole (**4g**) and 2-(3-cyanophenyl)-1-hydroxy-4-(pyridine-3-yl)-1*H*-imidazole (**5g**), respectively (**Scheme 2**).

The HPLC purity of all the synthesized compounds was over 97%. The structures were elucidated by MS, IR, ^{1}H NMR, and ^{13}C NMR spectra. All spectral data were in accordance with the assumed structures. In ESI-MS analysis, the target compounds showed $[M\text{-}OH+2H]^{+}$ ion peaks. The IR spectra of the target compounds displayed cyano stretching vibrations at 2223-2230 cm^{-1} and hydroxyl stretching vibrations at 3425-3429 cm^{-1}. In ^{1}H NMR spectra, the 1-hydroxy group of imidazole was observed as a broad singlet at approximately 12.79 ppm in series **4a-g** and 13.13 ppm in series **5a-g**, respectively.

2.2. Biological activity

The in vitro bovine XO inhibitory activity of compounds **4a–g** and **5a–g** was measured spectrophotometrically by determining uric acid production at 295 nm. Topiroxostat was included as a reference compound. The testing results are shown in **Table 1**.

As shown in **Table 1**, half of the synthesized compounds were effective and possessed micromolar level potency. Although the effects were much lower than that of the positive control Topiroxostat and compounds **1-3**, some interesting SAR information was obtained. In general, the **4a-g** series seemed to be more potent than the **5a-g** series overall. The majority of the compounds in the **4a-g** series were effective with IC_{50} values ranging from 0.64 to 15.42 μM. Meanwhile, compound **4f**, which linked an *iso*-pentyl for R_1 group, displayed the highest activity with an IC_{50} value of 0.64 μM, and was 10-fold more effective than its counterpart **5f** (IC_{50} = 6.73 μM). Additionally, a dose-dependent inhibition of XO by **4f** was exhibited (**Fig. 3**). Moreover, the ether tail at the 4′-position played a crucial role in the potency; its removal was accompanied by vanished potency (*e.g.*, **4a**, **4c**, **4e** and **4f** versus **4g**; **5b**, **5d** and **5f** versus **5g**). Furthermore, it can be found that from **4a** to **4c**, **4e** and **4f**, the inhibitory effects were enhanced 3.2-fold, 3.5-fold and 24-fold, respectively, which suggested that as the size of the ether tail at the 4′-position increased, the potency of the **4a-g** series was gradually enhanced (except **4b** and **4d)**.

In contrast, the **5a-g** series was less potent. Only three compounds (**5b**, **5d** and **5f**) were effective in this series, which suggested that the pyridine *para*-N of **4a-g** was much welcome than the pyridine *meta*-N of **5a-g**. This result was also supported by the isonicotinamide series in our previous studies [16]. In addition, compound **5f**, bearing an *iso*-pentyloxy at the 4′-position, exhibited relatively high potency with an IC_{50} value of 6.73 μM, which indicated that employment of an *iso*-pentyl as R_1 group improved the potency of both series, **4a-g** and **5a-g**.

2.3. Molecular modeling

To foresee the possible interactions of the synthesized compounds with XO and to rationalize the SARs observed in this study, molecular modeling simulations of Topiroxostat, **4f** and **5f** in the binding pocket of XO were performed. The simulations were carried out with Autodock 4 software package by a similar protocol to that reported in our previous study [30]. The crystal structure of bovine XO in complex with Febuxostat (PDB code: 1N5X) was adopted in docking calculations.

As shown in **Fig. 4**, the 1-hydroxy-2-phenyl-1*H*-imidazole moiety of **4f** and **5f** was located at a similar position in the XO active pocket and presented a set of similar interactions to compound **3** [30] such as the cyano group forming an H-bond with Asn768, the N-3 atom of imidazole accepting an H-bond from Glu802 and the ether tail being surrounded by some lipophilic amino acid residues, *e.g.*, Leu648 and Lys771. In particularly, the 1-hydroxy group formed an extra hydrogen bond with Thr1010 as expected. Moreover, the pyridine moiety of **4f** and **5f** could overlap with that of Topiroxostat in the active pocket [9]. However, an obvious difference between the docking models of **4f** and **5f** was that the pyridine *para*-N of **4f** formed an H-bond with Glu1261, just as Topiroxostat did; in contrast, *meta*-N of **5f** was absent from this interaction. This difference is consistent with their levels of inhibition potency.

2.4 3D-QSAR analysis

To further understand the structural basis of these compounds for XO inhibitory activity, we subsequently performed 3D-QSAR study using Topomer CoMFA method. The active compounds (*ie*, **4a**, **4c**, **4e**, **4f**, **5b**, **5d** and **5f**) were used in 3D-QSAR model building. In order to achieve a rational result, we

combined other published Topiroxostat-like compounds to perform this 3D-QSAR model, including 8 of 1,2,3-triazole derivatives (compounds **13-20**) synthesized in our previous studies [15] and 15 of 1,2,4-triazole derivatives (compounds **21-35**) reported by Sato T *et al* [14]. Therefore, The Topomer CoMFA study was carried out using a total of 30 compounds (**Table 2**), which randomly divided into training set and test set (marked with asterisk in **Table 2**) in the ratio of 5:1. Statistical parameters of the Topomer CoMFA model showed a reasonable cross-validated correlation coefficient q^2 of 0.885, indicating a good internal prediction ability of the model. The Topomer CoMFA model also exhibited a conventional correlation coefficient r^2 of 0.993 using 5 partial least-squares (PLS) components. The test set was used to evaluate the predictive ability of our developed model. The experimental and predicted values as well as their residuals from the training and test set molecules are listed in **Table 2**. The correlation between the predicted and experimental values of all compounds was plotted as shown in **Fig. 5**.

The results were analyzed and visualized using the standard deviation coefficient (StDev*Coeff) mapping option contoured by steric and electrostatic contributions [31]. The representative steric and electrostatic contour maps of compound **4f** derived from the Topomer CoMFA model are shown in **Fig. 6**. In **Fig. 6A**, one big green contour was found around the ether tail of compound **4f**, indicating that a steric substituent would be favored for R_1 group. This result could explain the gradually enhanced potency of compounds **4a**, **4c**, **4e** and **4f**. In **Fig. 6A** and **6B**, a small green contour and a blue contour near the 1-position of imidazole were observed, respectively, which indicated that an electropositive small steric bulky group would be helpful for activity in this area. Furthermore, a few red contours in **Fig. 6B** near the 3-position of imidazole suggested that an electronegative group at this position would be welcome; however, this position can't tolerate a bulky group according to several yellow contours in **Fig. 6A**. In **Fig. 6C**, a yellow contour was observed near the pyridine *para*-N of **4f**, meaning that substituent at this position

would be disfavored for potency. In **Fig. 6D**, one blue contour was observed at the *meta*-position of pyridine, indicating that the presence of positively charged group at this position may benefit the XO inhibitory potency.

2.5. Steady-state kinetic analysis

To further investigate the action mode of compounds **4a-g** with XO, enzyme kinetics studies of the representative compound **4f** were carried out (**Fig. 7**). Lineweaver-Burk plot analysis indicated that **4f** acted as a mixed-type inhibitor on XO. This behavior was distinct from Topiroxostat, but similar to hydroxy-topiroxostat, a metabolite of Topiroxostat with micromolar potency [32]. The different inhibition type may contribute to the decreased potency of **4f** compared with Topiroxostat.

3. Conclusions

In summary, we designed, synthesized and identified a series of 1-hydroxy-2-phenyl-4-pyridyl-1*H*-imidazole derivatives as novel XO inhibitors. Among them, compound **4f** was found to be the most promising derivative in the series with an IC_{50} value of 0.64 μM. The Lineweaver-Burk plot revealed that compound **4f** acted as a mixed-type XO inhibitor. SAR analysis indicated that the pyridine *para*-N atom played a crucial role in the inhibition, and an *iso*-pentyloxy group at the 4′-position improved the inhibitory potency. Molecular modeling provided a reasonable explanation for the SARs observed in this study and 3D-QSAR analysis explored the structural basis of these compounds. As a result, 1-hydroxy-2-phenyl-4-(pyridin-4-yl)-1*H*-imidazoles, especially compound **4f**, have good potential for further investigations.

4. Experimental protocols

4.1. Chemistry

Unless otherwise indicated, reagents and solvents were purchased from commercial sources and used without further purification. All reactions were monitored by TLC using silica gel aluminum cards (0.2 mm thickness) with fluorescent indicator 254 nm. The column chromatography was performed using silica gel (200-300 mesh) from Qingdao Ocean Chemicals (Qingdao, Shandong, China). The purity was determined by HPLC (Agilent 1260) by a C_{18} (250*4.6 mm, 5 μm) column with 0.02 M ammonium dihydrogen phosphate/acetonitrile (50: 50) as the mobile phase .The UV detection wavelength was 254 nm. Melting points were recorded on a YRT-3 melting apparatus and were uncorrected. ^{1}H NMR spectra were recorded on a Bruker 300 MHz spectrometer, a Bruker 400 MHz spectrometer or a Bruker 600 MHz spectrometer and ^{13}C NMR spectra were recorded on a Bruker 600 MHz spectrometer. Chemical shifts were expressed in parts per million using tetramethylsilane as an internal reference and $CDCl_3$ or DMSO-d_6 as the solvent. ESI-MS data were gathered using an Agilent 1100 instrument.

*4.1.1. Synthesis of 3-bromo-4-hydroxybenzaldehyde (**6**)*

A mixture of 4-hydroxybenzaldehyde (100.0 g, 0.82 mol) and iodine (5.2 g, 21 mmol) in dichloromethane (500 mL) was stirred at -5□ for 15 min, then a solution of bromine (138.0 g, 0.86 mol) in dichloromethane (300 mL) was slowly added dropwise to maintain the reactive temperature below 0□. After the completion of the addition, the mixture was reacted at room temperature for 24 h, then diluted

with 0.9% sodium bisulfite (1000 mL) and stirred for 30 min. The formed precipitate was collected by filtration, washed with water (100 mL) and dried to give 3-bromo-4-hydroxybenzaldehyde (133.0 g, yield 81.1%) as an off-white solid, which was used directly in the next step. MS (ESI) *m/z*: 198.9, 200.9 $[M-H]^-$. ^{1}H NMR (600 MHz, DMSO-d_6) δ 11.50 (s, 1H, OH), 9.77 (s, 1H, CHO), 8.02 (d, J = 2.0 Hz, 1H, Ar-H), 7.75 (dd, J = 2.0 & 8.4 Hz, 1H, Ar-H), 7.10 (d, J = 8.4 Hz, 1H, Ar-H).

*4.1.2. Synthesis of 4-benzoxy-3-bromobenzaldehyde (**7**)*

A mixture of 3-bromo-4-hydroxybenzaldehyde (133.0 g, 0.67 mol), benzyl bromide (125.1 g, 0.73 mol), anhydrous potassium carbonate (183.5 g, 1.33 mol) and potassium iodide (2.2 g, 0.013 mol) in DMF (700 mL) was reacted at 80□ for 8 h under nitrogen atmosphere. After that, the insoluble solid was filtered out and the filtrate was concentrated to remove near 2/3 of the solvent. The residue was diluted with ethyl acetate, washed with water and brine, dried over anhydrous Na_2SO_4 and evaporated in vacuum to afford 4-benzoxy-3-bromobenzaldehyde (174.4 g, yield 90.5%) as a slight yellow solid, which was directly used in the next step. MS (ESI) *m/z*: 291.0, 293.0 $[M+H]^+$. ^{1}H NMR (600 MHz, DMSO-d_6) δ 9.85 (s, 1H, CHO), 8.12 (d, J = 1.9 Hz, 1H, Ar-H), 7.92 (dd, J = 1.9 & 8.5 Hz, 1H, Ar-H), 7.49 (d, J = 7.5 Hz, 2H, Ar-H), 7.45 – 7.39 (m, 3H, Ar-H), 7.36 (t, J = 7.3 Hz, 1H, Ar-H), 5.35 (s, 2H, CH_2).

*4.1.3. Synthesis of 4-benzoxy-3-cyanobenzaldehyde (**8**)*

A mixture of 4-benzoxy-3-bromobenzaldehyde (93.0 g, 0.32 mol) and cuprous cyanide (37.2 g, 0.45 mol) in DMF (600 mL) was refluxed under nitrogen atmosphere for 6 h. The completed reaction was determined by TLC. The mixture was cooled to room temperature. Then, dichloromethane (500 mL) and ammonia (300 mL) were added. The oil layer was collected, successively washed with water and brine,

dried over anhydrous Na_2SO_4 and evaporated in vacuum to provide a crude product as a slight yellow solid, which was treated with methyl *tert*-butyl ether to yield 4-benzoxy-3-cyanobenzaldehyde as an off-white solid (56.9 g, yield 75%). MS (ESI) *m/z*: 238.1 $[M+H]^+$. ^{1}H NMR (600 MHz, DMSO-d_6) δ 9.89 (s, 1H, CHO), 8.32 (d, *J* = 1.9 Hz, 1H, Ar-H), 8.18 (dd, *J* = 1.9 & 8.8 Hz, 1H, Ar-H), 7.55 (d, *J* = 8.8 Hz, 1H, Ar-H), 7.50 (d, *J* = 7.4 Hz, 2H, Ar-H), 7.44 (t, *J* = 7.5 Hz, 2H, Ar-H), 7.38 (t, *J* = 7.3 Hz, 1H, Ar-H), 5.41 (s, 2H, CH_2).

*4.1.4. Synthesis of 5-formyl-2-hydroxybenzonitrile (**9**)*

A mixture of 4-benzoxy-3-cyanobenzaldehyde (10.0 g) and 10% Pd/C (0.50 g) in THF (40 mL) was stirred at room temperature for 4 h under hydrogen atmosphere. After the completion of the reaction, the Pd/C was filtered out and the filtrate was evaporated to give a slight yellow solid (5.0 g, yield 80%). ^{1}H NMR (600 MHz, DMSO-d_6) δ 11.51 (s, 1H, OH), 9.77 (s, 1H, CHO), 8.04 (d, *J* = 1.8 Hz, 1H, Ar-H), 7.75 (dd, *J* = 1.8 & 8.4 Hz, 1H, Ar-H), 7.11 (d, *J* = 8.4 Hz, 1H, Ar-H).

4.1.5. *5-Formyl-2-methoxybenzonitrile (**10a**).*

Into a mixture of 5-formyl-2-hydroxybenzonitrile (8.0 g, 0.04 mol) and anhydrous potassium carbonate (11.0 g, 0.08 mol) in DMF (20 mL), dimethyl sulfate (5.6 g, 0.044 mol) in DMF (20 mL) was slowly added dropwise at 0□. The resulting mixture was stirred at room temperature for 5 h, then poured into water (40 mL) and stirred for 15 min. the resulting solid was filtered, washed with water and dried to give 3-cyano-4-methoxybenzonitrile (7.0 g, 79.4%) as a white solid. mp 70.5–72.3 °C. ^{1}H NMR (300 MHz, $CDCl_3$) δ 9.88 (s, 1H, CHO), 8.10 (d, 1H, *J* = 2.0 Hz, Ar-H), 8.06 (dd, 1H, *J* = 2.1 & 8.8 Hz, Ar-H), 7.10 (d, 1H, *J* = 8.7 Hz, Ar-H), 3.85 (s, 3H, OCH_3).

*4.1.6. General procedure for the synthesis of 2-alkoxy-5-formylbenzonitriles **10b-10f***

A mixture of 5-formyl-2-hydroxybenzonitrile (0.04 mol), alkyl chloride or alkyl bromide (0.05 mol) and anhydrous potassium carbonate (0.08 mol) in DMF (40 mL) was reacted at 80□ for 6 h under nitrogen atmosphere. After that, 2/3 of the solvent was removed by evaporation in vacuum. Then, water (40 mL) and ethyl acetate (40 mL) were added. The organic layer was collected, washed with brine, dried over anhydrous Na_2SO_4 to yield the corresponding 2-alkoxy-5-formylbenzonitriles **10b-10f**.

4.1.6.1. *2-(Allyloxy)-5-formylbenzonitrile (**10b**)*

A slight yellow oil, yield 90.4%. ^{1}H NMR (600 MHz, DMSO-d_6) δ 9.88 (s, 1H), 8.29 (d, J = 2.0 Hz, 1H), 8.15 (dd, J = 8.8 & 2.1 Hz, 1H), 7.44 (d, J = 8.8 Hz, 1H), 6.07 (m, 1H), 5.48 (dd, J = 17.3 & 1.6 Hz, 1H), 5.35 (dd, J = 10.6 & 1.4 Hz, 1H), 4.96 – 4.79 (m, 2H).

4.1.6.2. *5-Formyl-2-isopropoxybenzonitrile (**10c**)*

A slight yellow solid, yield 82.4%. Mp 51.5–52.6 °C. ^{1}H NMR (300 MHz, $CDCl_3$) δ 9.88 (s, 1H, CHO), 8.09 (d, 1H, J = 2.0 Hz, Ar-H), 8.05 (dd, 1H, J = 2.1 & 8.7 Hz, Ar-H), 7.10 (d, 1H, J = 8.8 Hz, Ar-H), 4.80 (m, 1H, OCH), 1.46 (d, 6H, J = 6.1 Hz, $2CH_3$).

4.1.6.3. *5-Formyl-2-isobutoxybenzonitrile (**10d**)*

A yellow oil, yield 93.2%. ^{1}H NMR (300 MHz, $CDCl_3$) δ 9.89 (s, 1H, CHO), 8.10 (d, 1H, J = 2.0 Hz, Ar-H), 8.06 (dd, 1H, J = 2.1 & 8.7 Hz, Ar-H), 7.09 (d, 1H, J = 8.7 Hz, Ar-H), 3.95 (t, 2H, J = 6.5 Hz, OCH_2), 2.22 (m, 1H, CH), 1.01 (d, 6H, J = 6.8, $2CH_3$).

4.1.6.4. *2-(sec-Butoxy)-5-formylbenzonitrile (**10e**)*

A yellow oil, yield 90.5%. ^{1}H NMR (300 MHz, $CDCl_3$) δ 9.88 (s, 1H, CHO), 8.09 (d, 1H, J = 1.8 Hz, Ar-H), 8.04 (dd, 1H, J = 1.8 & 8.8 Hz, Ar-H), 7.09 (d, 1H, J = 8.8 Hz, Ar-H), 4.56 (m, 1H, OCH), 1.79 (m, 2H, CH_2), 1.41 (d, 3H, J = 6.1 Hz, CH_3), 1.01 (t, 3H, J = 7.4, CH_3).

4.1.6.5. *5-Formyl-2-isopentyloxybenzonitrile (**10f**)*

A yellow solid, yield 87.8%., mp 47.1–48.5°C. ^{1}H NMR (300 MHz, $CDCl_3$) δ 9.90 (s, 1H, CHO), 8.09 (s, 1H, Ar-H), 8.06 (d, 1H, J = 8.8 Hz, Ar-H), 7.11 (d, 1H, J = 8.8 Hz, Ar-H), 4.21 (t, 2H, J = 6.5 Hz, OCH_2), 1.91 (m, 1H, CH), 1.80 (m, 2H, CH_2), 1.00 (d, 6H, J = 6.6, $2CH_3$).

*4.1.7. Synthesis of 2-oxo-2-(pyridin-4-yl)acetaldehyde oxime (**11**)*

Into a sodium ethoxide solution prepared by dissolving the metal sodium (4.0 g, 0.18 mol) in anhydrous ethanol (100 mL), 4-acetylpyridine (20.0 g, 0.17 mol) was added. The solution was stirred at -5□ for 15 min, and then *tert*-butyl nitrite (21.9 g, 0.22 mol) was added dropwise. The reactive solution was stirred at 0-10□ for 24 h then frozen in the fridge for 24 h. The generated precipitate was collected by filtration to provide a red solid (4.1 g, yield 82.0%). MS (ESI) *m/z*: 149.1 $[M-H]^-$.

*4.1.8. Synthesis of 2-oxo-2-(pyridin-3-yl)acetaldehyde oxime (**12**)*

2-Oxo-2-(pyridin-3-yl)acetaldehyde oxime was synthesized by a procedure similar to that for the preparation of 2-oxo-2-(pyridin-4-yl)acetaldehyde oxime with 3-acetylpyridine instead of 4-acetylpyridine. A slight red solid (yield 78.0%). MS (ESI) *m/z*: 149.1 $[M-H]^-$.

*4.1.9. General procedure for the synthesis of 2-(4-alkoxy-3-cyanobenzyl)-1-hydroxy-4-(pyridin-4-yl)-1H-imidazoles **4a-4g** and 2-(4-alkoxy-3-cyanobenzyl)-1-hydroxy-4-(pyridin-3-yl)-1H-imidazoles **5a-5g***

A mixture of 4-alkoxy-3-cyanobenzaldehyde (0.015 mol) and ammonium acetate (0.15 mol) in methanol (30 mL) was added 2-oxo-2-(pyridin-4-yl)acetaldehyde oxime (0.018 mol) or 2-oxo-2-(pyridin-3-yl)acetaldehyde oxime (0.018 mol) for the synthesis of **4a-4g** and **5a-5g**, respectively. The mixture was refluxed for 24 h under nitrogen atmosphere. The solvent was evaporated in vacuum and the residue was treated with ethyl acetate (50 mL) and water (50 mL). The oil layer was separated and washed with brine, dried over anhydrous Na_2SO_4 and evaporated in vacuum to obtain a crude product, which was purified by column chromatography (petroleum ether: ethyl acetate = 1:1) to obtain the corresponding **4a-4g** and **5a-5g.**

4.1.9.1. *2-(3-Cyano-4-methoxybenzyl)-1-hydroxy-4-(pyridin-4-yl)-1H-imidazole (**4a**)*

A yellow solid (0.9 g, yield 21.4%). HPLC 98.2%. Mp 206.0□-208.6 □. MS (ESI) *m/z*: 277.1 $[M\text{-}OH+2H]^+$; ^{1}H NMR (400 MHz, DMSO-d_6) δ 12.91 (s, 1H, NOH), 8.53 (s, 2H, Py-H), 8.27 (m, 2H, Ar-H), 8.07 (s, 1H, Imidazole-H),7.79 (s, 2H, Py-H), 7.40 (s, 1H, Ar-H), 3.97 (s, 3H, CH_3); ^{13}C NMR (150 MHz, DMSO-d_6) δ 160.73, 149.84, 144.86, 141.43, 138.58, 131.66, 129.89, 123.53, 118.79, 117.53, 116.09, 112.92, 100.71, 56.60; IR (KBr, cm^{-1}) 3426.6, 2921.9, 2851.5, 2224.5, 1608.4.

4.1.9.2. *2-(4-Allyl-3-cyanobenzyl)-1-hydroxy-4-(pyridin-4-yl)-1H-imidazole (**4b**)*

A yellow solid, yield 26.7%. HPLC 98.2%. Mp 216.0 □-218.6 □. MS (ESI) *m/z*: 303.1 $[M\text{-}OH+2H]^+$;

^{1}H NMR (400 MHz, DMSO-d_6) δ 12.92 (s, 1H, NOH), 8.54 (d, 2H, J = 4.0 Hz, Py -H), 8.29 (m, 2H, Ar-H), 8.08 (s, 1H, Imidazole-H), 7.79 (d, 2H, J = 4.0 Hz, Py-H), 7.41 (d, 1H, J = 8.0 Hz, Ar-H), 6.10 (m, 1H, –CH=CH_2), 5.51 (m, 1H, –CH=CH_2), 5.46 (m, 1H, –CH=CH_2), 4.48 (d, 2H, J = 4.0 Hz, OCH_2); ^{13}C NMR (150 MHz, DMSO-d_6) δ 159.71, 149.99, 145.47, 141.16, 137.52, 133.66, 132.59, 131.89, 130.27, 123.97, 118.36, 116.26, 115.02, 113.96, 101.17, 69.47; IR (KBr, cm^{-1}) 3426.7, 3078.9, 2920.0, 2230.5, 1607.1.

4.1.9.3. *2-(3-Cyano-4-isopropoxybenzyl)-1-hydroxy-4-(pyridin-4-yl)-1H-imidazole (**4c**)*

A yellow solid, yield 19.4%. HPLC 98.6%. Mp 202.3 □-205.2 □. MS (ESI) *m/z*: 305.1 [M-OH+2H]$^{+}$; ^{1}H NMR (400 MHz, DMSO-d_6) δ 13.09 (s, 1H, NOH), 8.56 (d, 2H, J = 5.1 Hz, Py-H), 8.27 (m, 2H, Ar-H), 8.09 (s, 1H, Imidazole-H),7.84 (d, 2H, J = 5.3 Hz, Py-H), 7.43 (d, 1H, J = 8.8 Hz, Ar-H), 4.89 (m, 1H, CH), 1.37 (d, 6H, J = 6.0 Hz, $2CH_3$); ^{13}C NMR (150 MHz, DMSO-d_6) δ 159.22, 149.85, 144.91, 141.44, 138.56, 131.56, 130.02, 123.26, 118.78, 117.51, 116.21, 114.73, 101.71, 71.73, 21.61; IR (KBr, cm^{-1}) 3429.1, 3046.4, 2923.7, 2224.3, 1607.1.

4.1.9.4. *2-(3-Cyano-4-isobutoxybenzyl)-1-hydroxy-4-(pyridin-4-yl)-1H-imidazole (**4d**)*

A yellow solid, yield 24.6%. HPLC 97.6%. Mp 243.0 □-244.7 □. MS (ESI) *m/z*: 319.2 [M-OH+2H]$^{+}$; ^{1}H NMR (400 MHz,DMSO-d_6) δ 12.89 (s, 1H, NOH), 8.54 (d, 2H, J = 4.0 Hz, Py-H), 8.27 (m, 2H, Ar-H), 8.06 (s, 1H, Imidazole-H), 7.79 (d, 2H, J = 4.0 Hz, Py-H), 7.39 (d, 1H, J = 8.0 Hz, Ar-H), 3.98 (d, 2H, CH_2), 2.12 (m, 1H, CH), 1.03 (d, 6H, J = 8.0 Hz, $2CH_3$); ^{13}C NMR (150 MHz, DMSO-d_6) δ 160.22, 149.88, 144.94, 141.40, 138.56, 131.65, 129.83, 123.40, 118.76, 117.52, 115.97, 113.69, 100.95, 74.89, 27.62, 18.75; IR (KBr, cm^{-1}) 3425.4, 2956.3, 2852.6, 2227.9, 1607.2.

4.1.9.5. *2-(4-(sec-Butoxy) 3-cyanobenzyl)-1-hydroxy-4-(pyridin-4-yl)-1H-imidazole (**4e**)*

A yellow solid, yield 21.4%. HPLC 98.2%. Mp 184.7 □-191.0 □. MS (ESI) *m/z*: 319.1 $[M-OH+2H]^+$; ^{1}H NMR (400 MHz, DMSO-d_6) δ 12.90 (s, 1H, NOH), 8.54 (d, 2H, *J* = 4.0 Hz, Py-H), 8.26 (m, 2H, Ar-H), 8.07 (s, 1H, Imidazole-H), 7.79 (d, 2H, *J* = 4.0 Hz, Py-H), 7.43 (d, 1H, *J* = 8.0 Hz, Ar-H), 4.69 (m, 1H, CH), 1.73 (m, 2H, CH_2), 1.32 (d, 3H, *J* = 8.0 Hz, CH_3), 0.98 (t, 3H, *J* = 8.0 Hz, CH_3); ^{13}C NMR (150 MHz, DMSO-d_6) δ 159.54, 149.84, 145.02, 141.46, 138.56, 131.61, 130.04, 128.64, 123.24, 118.73, 116.16, 114.71, 101.71, 76.39, 28.40, 18.82, 9.20; IR (KBr, cm^{-1}) 3426.7, 3094.7, 2924.0, 2227.5, 1605.9.

4.1.9.6. *2-(3-Cyano-4-isopentyloxybenzyl)-1-hydroxy-4-(pyridin-4-yl)-1H-imidazole (**4f**)*

A yellow solid, yield 19.4%. HPLC 98.3%. Mp 148.6 □-152.0 □. MS (ESI) *m/z*: 333.1 $[M-OH+2H]^+$; ^{1}H NMR (400 MHz, DMSO-d_6) δ 12.92 (s, 1H, NOH), 8.53 (s, 2H, Py-H), 8.27 (s, 2H, Ar-H), 8.07 (s, 1H, Imidazole-H), 7.79 (s, 2H, Py-H), 7.41 (d, 1H, *J* = 8.0 Hz, Ar-H), 4.21 (m, 2H, CH_2), 1.82 (m, 1H, CH), 1.68 (m, 2H, CH_2), 0.96 (d, 6H, *J* = 8.0 Hz, $2CH_3$); ^{13}C NMR (150 MHz, DMSO-d_6) δ 160.13, 149.83, 144.91, 141.45, 138.57, 131.57, 129.86, 123.38, 118.78, 117.48, 116.04, 113.58, 100.92, 67.60, 37.02, 24.61, 22.36; IR (KBr, cm^{-1}) 3425.4, 2956.3, 2923.1, 2227.9, 1607.2.

4.1.9.7. *2-(3-Cyanobenzyl)-1-hydroxy-4-(pyridin-4-yl)-1H-imidazole (**4g**)*

A slight yellow solid, yield 15.4%, HPLC 97.2%. Mp: 208.6□. -209.8 □. MS (ESI) *m/z*: 246.9 $[M-OH+2H]^+$; ^{1}H NMR (400 MHz,DMSO-d_6) δ 13.13 (s,1H, NOH), 8.55 (d, 2H, *J* = 4.4 Hz, Py-H), 8.39 (s, 1H, Ar-H), 8.34 (d, 1H, *J* = 7.9 Hz Ar-H), 8.16 (s, 1H, Imidazole-H), 7.87 (d, 1H, *J* = 7.6 Hz, Ar-H), 7.82 (d, 2H, *J* = 5.1 Hz, Py-H), 7.73 (t, 1H, *J* = 7.8 Hz, Ar-H); ^{13}C NMR (150 MHz, DMSO-d_6) δ 149.93, 144.75, 141.28, 139.04, 131.76, 131.24, 130.20, 129.53, 128.32, 118.85, 118.53, 118.23, 112.02; IR (KBr,

cm^{-1}) 3429.2, 3073.9, 3041.8, 2231.5, 1605.0.

4.1.9.8. *2-(3-Cyano-4-methoxybenzyl)-1-hydroxy-4-(pyridin-3-yl)-1H-imidazole (**5a**)*

A yellow solid, yield 15.4%. HPLC 97.2%. Mp 199.9 □-204.2 □. MS (ESI) *m/z*: 277.1 $[M\text{-}OH+2H]^+$; ^1H NMR (400 MHz, DMSO-d_6) δ 12.94 (s, 1H, NOH), 9.06 (s, 1H, Py-H), 8.42 (d, 1H, *J* = 3.1 Hz, Py -H), 8.31 (m, 2H, Ar-H), 8.19 (m, 1H, Py-H), 7.88(s, 1H, Imidazole-H), 7.40 (m, 2H, Ar-H & Py-H), 3.97 (s, 3H, CH_3); ^{13}C NMR (150 MHz, DMSO-d_6) δ 160.62, 147.30, 145.84, 144.73, 137.54, 131.61, 131.35, 130.09, 129.79, 123.70, 123.66, 116.12, 114.53, 112.90, 100.68, 56.58; IR (KBr, cm^{-1}) 3420.4, 3104.4, 2922.9, 2227.9, 1602.2.

4.1.9.9. *2-(4-Allyloxy-3-cyanobenzyl)-1-hydroxy-4-(pyridin-3-yl)-1H-imidazole (**5b**)*

A yellow solid, yield 19.4%. HPLC 97.8%. Mp 212.3 □-215.2 □. MS (ESI) *m/z*: 303.1 $[M\text{-}OH+2H]^+$; ^1H NMR (400 MHz, DMSO-d_6) δ 12.81 (s, 1H, NOH), 9.06 (d, 1H, *J* = 2.2 Hz, Py-H), 8.43 (dd, 1H, *J* = 1.7 Hz & 4.8 Hz, Py-H), 8.29 (d, 1H, *J* = 2.2 Hz, Ar-H), 8.25 (dd, 1H, *J* = 2.3 Hz & 8.8 Hz, Ar-H), 8.19 (m, 1H, Py-H), 7.88 (s, 1H, Imidazole-H), 7.40 (m, 2H, Ar-H & Py-H), 6.09 (m, 1H, $\underline{CH}=CH_2$), 5.51 (dd, 1H, *J* = 1.7 Hz &17.2 Hz, -CH=$\underline{CH_2}$), 5.36 (dd, 1H, *J* = 1.6 Hz & 14.1 Hz, -CH=$\underline{CH_2}$), 4.80 (d, 2H, *J* = 5.2 Hz, OCH_2); ^{13}C NMR (150 MHz, DMSO-d_6) δ 159.50, 147.30, 145.84, 144.71, 137.30, 132.49, 131.46, 131.35, 129.82, 129.61, 123.81, 123.66, 118.21, 116.07, 114.51, 113.92, 101.04, 69.33; IR (KBr, cm^{-1}) 3428.5, 3082.0, 2964.0, 2227.4, 1601.3.

4.1.9.10. *2-(3-Cyano-4-isopropoxybenzyl)-1-hydroxy-4-(pyridin-3-yl)-1H-imidazole (**5c**)*

A yellow solid, yield 12.4%. HPLC 98.5%. Mp 202.3 □-205.2 □. MS (ESI) *m/z*: 305.0 $[M\text{-}OH+2H]^+$;

^{1}H NMR (400 MHz, DMSO-d_6) δ 12.80 (s, 1H, NOH), 9.07 (s, 1H, Py-H),8.43 (d, 1H, J = 3.8 Hz, Py-H), 8.27 (m, 2H, Ar-H), 8.19 (d, 1H, J = 7.7 Hz, Py-H), 7.92 (s, 1H, Imidazole-H), 7.41 (d, 2 Hz, J = 8.0 Hz, Ar-H), 7.43 (m, 2H, Ar-H & Py-H), 4.80 (m, 1H, CH), 1.36 (d, 6H, J = 6.0 Hz, 2CH_3); ^{13}C NMR (150 MHz, DMSO-d_6) δ 159.12, 147.28, 145.82, 144.80, 137.27, 131.52, 131.38, 129.94, 129.72, 123.68, 123.42, 117.42, 116.26, 114.71, 101.71, 71.72, 21.62; IR (KBr, cm^{-1}) 3425.9, 3098.4, 2922.3, 2227.9, 1617.4.

4.1.9.11. *2-(3-Cyano-4-isobutoxybenzyl)-1-hydroxy-4-(pyridin-3-yl)-1H-imidazole (**5d**).*

A yellow solid, yield 20.1%. HPLC 97.3%. Mp 191.6 □-195.8 □. MS (ESI) *m/z*: 319.1 $[M\text{-}OH+2H]^+$; ^{1}H NMR (400 MHz, DMSO-d_6) δ 12.80 (s, 1H, NOH), 9.06 (s, 1H, Py-H), 8.42 (d, 1H, J = 4.7 Hz, Py-H), 8.27 (m, 2H, Ar-H), 8.19 (d, 1H, J = 8.0 Hz, Py-H), 7.90 (s, 1H, Imidazole-H), 7.42 (m, 2H, Ar-H & Py-H), 3.98 (d, 2H, J = 6.4 Hz, CH_2), 2.10 (m, 1H, CH), 1.03 (d, 6H, J = 6.6 Hz, 2CH_3); ^{13}C NMR (150 MHz, DMSO-d_6) δ 160.09, 147.30, 145.85, 144.70, 138.13, 131.55, 131.33, 130.09, 129.70, 123.65, 123.58, 116.01, 115.43, 113.64, 100.92, 74.87, 27.62, 18.74; IR (KBr, cm^{-1}) 3427.1, 2960.7, 2921.7, 2229.4, 1621.0.

4.1.9.12. *2-(4-(sec-Butoxy)-3-cyanobenzyl)-1-hydroxy-4-(pyridin-3-yl)-1H-imidazole (**5e**)*

A yellow solid, yield 16.7%. HPLC 98.4%. Mp 195.1 □-197.9 □. MS (ESI) *m/z*: 319.1 $[M\text{-}OH+2H]^+$; ^{1}H NMR (400 MHz, DMSO-d_6) δ 12.80 (s, 1H, NOH), 9.06 (s, 1H, Py-H), 8.42 (s, 1H,Py -H), 8.27 (m, 2H, Ar-H), 8.19 (d, 1H, J = 8.0 Hz, P y-H), 7.91 (s, 1H, Imidazole-H), 7.39 (m, 2H, Ar-H & Py-H), 4.69 (m, 1H, CH), 1.74 (m, 2H, CH_2), 1.32 (d, 3H, J = 6.0 Hz, CH_3), 0.97 (t, 3H, J = 6.0 Hz, CH_3); ^{13}C NMR (150 MHz, DMSO-d_6) δ 159.47, 147.05, 145.63, 144.85, 136.54, 131.76, 131.72, 130.22, 129.62, 123.79,

123.34, 117.28, 116.23, 114.66, 101.70, 76.40, 28.44, 18.86, 9.23; IR (KBr, cm^{-1}) 3425.3, 2963.2, 2922.2, 2227.1, 1620.0.

4.1.9.13. *2-(3-Cyano-4-isopentyloxybenzyl)-1-hydroxy-4-(pyridin-3-yl)-1H-imidazole (**5f**)*

A yellow solid, yield 12.1%. HPLC 97.9%. Mp 197.3 □-203.9 □. MS (ESI) *m/z*: 333.1 $[M\text{-}OH+2H]^+$; ^1H NMR (400 MHz, DMSO-d_6) δ 12.80 (s, 1H, NOH), 9.07 (s, 1H, Py-H), 8.42 (s, 1H, Py–H), 8.26 (m, 2H, Ar-H), 8.19 (d, 1H, *J* = 7.9 Hz, Py-H), 7.89 (s, 1H, Imidazole-H), 7.39 (m, 2H, Ar-H & Py-H), 4.19 (t, 2H, *J* = 6.5 Hz, CH_2), 1.83 (m, 1H, CH), 1.67 (q, 2H, *J* = 6.5 Hz, CH_3), 0.95 (d, 6H, *J* = 6.6 Hz, $2CH_3$); ^{13}C NMR (150 MHz, DMSO-d_6) δ 160.02, 147.24, 145.79, 144.77, 137.42, 131.53, 131.37, 129.76, 129.58, 123.66, 123.53, 117.07, 116.07, 113.58, 100.90, 67.58, 37.03, 24.61, 22.37; IR (KBr, cm^{-1}) 3425.5, 2956.4, 2922.0, 2228.4, 1620.7.

4.1.9.14. *2-(3-Cyanobenzyl)-1-hydroxy-4-(pyridin-3-yl)-1H-imidazole (**5g**)*

A yellow solid, yield 21.3%. HPLC 97.1%. Mp 222.2 □-226.9 □. MS (ESI) *m/z*: 246.9 $[M\text{-}OH+2H]^+$; ^1H NMR (400 MHz, DMSO-d_6) δ 13.04 (s, 1H, NOH), 9.09 (s, 1H, Py-H), 8.44 (d, 1H, *J* = 4.7 Hz, Py-H), 8.38 (s, 1H, Ar-H), 8.33 (d, 1H, *J* = 8.0 Hz, Py-H), 8.21 (d, 1H, *J* = 8.0 Hz, Ar-H), 8.01 (s, 1H, Imidazole-H), 7.86 (m, 1H, Py -H), 7.73 (t, 1H, Ar-H), 7.43 (m, 1H, Py -H); ^{13}C NMR (150 MHz, DMSO-d_6) δ 147.48, 145.91, 144.52, 131.59, 131.47, 131.38, 130.20, 129.43, 128.19, 127.25, 123.70, 118.55, 116.36, 114.52, 111.98; IR (KBr, cm^{-1}) 3428.8, 2923.4, 2853.7, 2226.6, 1632.6.

4.2. Assay of in vitro XO inhibitory activity

Bovine XO inhibitory potency in vitro was assayed spectrophotometrically by measuring uric acid formation at 295 nm at 25°C. The testing method was based on the procedure reported by Matsumoto *et al.* [32] with modification. The assay mixture contained 0.1 M sodium pyrophosphate buffer (pH 8.3), 0.3 mM Na_2EDTA, 64 μM xanthine, 15 U/L XO (Sigma, X4875), and the test compound. The XO inhibition by various compounds was measured by the reduction of the uric acid concentration. The enzyme needed pre-incubation for 15 min with the test compound, and the reaction was started by addition of xanthine. Topiroxostat was used as a positive control. All the tests were performed in triplicate. Compounds presenting inhibitory effects over 50% at the concentration of 10 μg/mL were further tested at a wide range of concentrations to calculate their IC_{50} value by using SPSS 20.0 software.

4.3. Molecular modeling

AutoDock 4 [33] was used to perform docking calculations. The crystal structure of bovine XO in complex with Febuxostat (PDB code: 1N5X) [8] was adopted in docking simulations. An 80 × 80 × 80 Å grid box with a grid spacing of 0.375 Å was generated to define the binding pocket. Affinity grid fields were generated using the auxiliary program AutoGrid 4. Ligand structures were built and minimized with Accelrys Discovery Studio 3.0 software package. Flexible torsions in the ligands were assigned, and all dihedral angles were allowed to freely rotate.

The Lamarckian genetic algorithm was used to determine the appropriate binding positions, orientations, and conformations of ligands [33]. All other parameters were maintained as default. In each group, the lowest binding energy configuration with the highest percentage frequency was selected as the group representative.

4.4. 3D-QSAR analysis

In this study, 30 of Topiroxostat-like compounds were used to conduct 3D-QSAR model with Topomer CoMFA method, including 7 of imidazole derivatives synthesized in this work, 8 of 1,2,3-triazole derivatives reported in our previous studies [15] and 15 of 1,2,4-triazole derivatives reported by Sato T *et al* [14]. The structures of compounds and their biological data in the form of pIC_{50} are listed in **Table 2**. The 3D structures were prepared using Sybyl X-1.1. The Gasteiger-Hückel charge was applied to each molecule and energy minimization was performed using the Tripos force field [34, 35]. The 30 compounds were divided into the training set (25 compounds) and the test set (5 compounds) in the ratio of 5:1. The training set was used to build the 3D-QSAR model, and the test set was used to test the predictions of the model [36]. Each molecule in training set was divided into two sets of fragments shown as S1 and S2 groups (**Fig. 6**). A carbon sp^3 probe was applied for calculating steric and electrostatic parameters. PLS regression was used to generate the Topomer CoMFA model.

Acknowledgments

This work was supported by Program for Liaoning Excellent Talents in University (LR2012035) and the Scientific Research Program of Hainan Province (ZDYF2016143).

References

[1] M. Gliozzi, N. Malara, S. Muscoli, V. Mollace, The treatment of hyperuricemia, Int. J. Cardiol. 213 (2016) 23-27.

[2] A. Šmelcerović, K. Tomović, Ž. Šmelcerović, Ž. Petronijević, G. Kocić, T. Tomašič, Ž. Jakopin, M. Anderluh, Xanthine oxidase inhibitors beyond allopurinol and febuxostat; an overview and selection of potential leads based on in silico calculated physico-chemical properties, predicted pharmacokinetics and toxicity, Eur. J. Med. Chem. 135 (2017) 491-516.

[3] M.V. Rodrigues, A.F. Barbosa, J.F. da Silva, D.A. dos Santos, K.L. Vanzolini, M.C. de Moraes, A.G. Correa, Q.B. Cass, 9-Benzoyl 9-deazaguanines as potent xanthine oxidase inhibitors, Bioorg. Med. Chem. 24 (2016) 226-231.

[4] J.-M. Lü, Q. Yao, C. Chen, 3,4-Dihydroxy-5-nitrobenzaldehyde (DHNB) is a potent inhibitor of xanthine oxidase: A potential therapeutic agent for treatment of hyperuricemia and gout, Biochem. Pharmacol. 86 (2013) 1328-1337.

[5] Z. Smelcerovic, A. Veljkovic, G. Kocic, D. Yancheva, Z. Petronijevic, M. Anderluh, A. Smelcerovic, Xanthine oxidase inhibitory properties and anti-inflammatory activity of 2-amino-5-alkylidene-thiazol-4-ones, Chem.-Biol. Interact. 229 (2015) 73-81.

[6] H. Singh, S. Sharma, R. Ojha, M.K. Gupta, K. Nepali, P.M.S. Bedi, Synthesis and evaluation of naphthoflavones as a new class of non purine xanthine oxidase inhibitors, Bioorg. Med. Chem. Lett. 24 (2014) 4192-4197.

[7] P. Pacher, Therapeutic Effects of Xanthine Oxidase Inhibitors: Renaissance Half a Century after the Discovery of Allopurinol, Pharmacol. Rev. 58 (2006) 87-114.

[8] K. Okamoto, B.T. Eger, T. Nishino, S. Kondo, E.F. Pai, An extremely potent inhibitor of xanthine oxidoreductase. Crystal structure of the enzyme-inhibitor complex and mechanism of inhibition, J. Biol. Chem. 278 (2002) 1848-1855.

[9] E. Cristofer, T.E. Bryan, O. Ken, N. Tomoko, N. Takeshi, F.P. Emil, Crystal structures of bovine milk xanthine dehydrogenase and xanthine oxidase: Structure-based mechanism of conversion, PNAS 97 (2000) 10723-10728.

[10] S. Ishibuchi, H. Morimoto, T. Oe, T. Ikebe, H. Inoue, A. Fukunari, M. Kamezawa, I. Yamada, Y. Naka, Synthesis and structure–activity relationships of 1-Phenylpyrazoles as xanthine oxidase inhibitors, Bioorg. Med. Chem. Lett. 11 (2001) 879-882.

[11] Q. Guan, Z. Cheng, X. Ma, L. Wang, D. Feng, Y. Cui, K. Bao, L. Wu, W. Zhang, Synthesis and bioevaluation of 2-phenyl-4-methyl-1,3-selenazole-5-carboxylic acids as potent xanthine oxidase inhibitors, Eur. J. Med. Chem. 85 (2014) 508-516.

[12] T.J. Zhang, Q.X. Wu, S.Y. Li, L. Wang, Q. Sun, Y. Zhang, F.H. Meng, H. Gao, Synthesis and evaluation of 1-phenyl-1H-1,2,3-triazole-4-carboxylic acid derivatives as xanthine oxidase inhibitors, Bioorg. Med. Chem. Lett. 27 (2017) 3812-3816.

[13] J.U. Song, S.P. Choi, T.H. Kim, C.-K. Jung, J.-Y. Lee, S.-H. Jung, G.T. Kim, Design and synthesis of novel 2-(indol-5-yl)thiazole derivatives as xanthine oxidase inhibitors, Bioorg. Med. Chem. Lett. 25 (2015) 1254-1258.

[14] T. Sato, N. Ashizawa, T. Iwanaga, H. Nakamura, K. Matsumoto, T. Inoue, O. Nagata, Design, synthesis, and pharmacological and pharmacokinetic evaluation of 3-phenyl-5-pyridyl-1,2,4-triazole derivatives as xanthine oxidoreductase inhibitors, Bioorg. Med. Chem. Lett. 19 (2009) 184-187.

[15] T.J. Zhang, S.Y. Li, Y. Zhang, Q.X. Wu, F.H. Meng, Design, synthesis, and biological evaluation of

5-(4-(pyridin-4-yl)-1H-1,2,3-triazol-1-yl)benzonitrile derivatives as xanthine oxidase inhibitors, Chem. Biol. Drug Des. 00 (2017) 1-8. 10.1111/cbdd.13114.

[16] T.J. Zhang, S.Y. Li, L. Wang, Q. Sun, Q.X. Wu, Y. Zhang, F.H. Meng, Design, synthesis and biological evaluation of N-(4-alkoxy-3-cyanophenyl)isonicotinamide/nicotinamide derivatives as novel xanthine oxidase inhibitors, Eur. J. Med. Chem. 141 (2017) 362-372.

[17] C. B-Rao, A. Kulkarni-Almeida, K.V. Katkar, S. Khanna, U. Ghosh, A. Keche, P. Shah, A. Srivastava, V. Korde, K.V.S. Nemmani, N.J. Deshmukh, A. Dixit, M.K. Brahma, U. Bahirat, L. Doshi, R. Sharma, H. Sivaramakrishnan, Identification of novel isocytosine derivatives as xanthine oxidase inhibitors from a set of virtual screening hits, Bioorg. Med. Chem. 20 (2012) 2930-2939.

[18] S. Khanna, S. Burudkar, K. Bajaj, P. Shah, A. Keche, U. Ghosh, A. Desai, A. Srivastava, A. Kulkarni-Almeida, N.J. Deshmukh, A. Dixit, M.K. Brahma, U. Bahirat, L. Doshi, K.V.S. Nemmani, P. Tannu, A. Damre, C. B-Rao, R. Sharma, H. Sivaramakrishnan, Isocytosine-based inhibitors of xanthine oxidase: Design, synthesis, SAR, PK and in vivo efficacy in rat model of hyperuricemia, Bioorg. Med. Chem. Lett. 22 (2012) 7543-7546.

[19] K. Bajaj, S. Burudkar, P. Shah, A. Keche, U. Ghosh, P. Tannu, S. Khanna, A. Srivastava, N.J. Deshmukh, A. Dixit, Y. Ahire, A. Damre, K.V.S. Nemmani, A. Kulkarni-Almeida, C. B-Rao, R. Sharma, H. Sivaramakrishnan, Lead optimization of isocytosine-derived xanthine oxidase inhibitors, Bioorg. Med. Chem. Lett. 23 (2013) 834-838.

[20] J. Evenäs, F. Edfeldt, M. Lepistö, N. Svitacheva, A. Synnergren, B. Lundquist, M. Gränse, A. Rönnholm, M. Varga, J. Wright, M. Wei, S. Yue, J. Wang, C. Li, X. Li, G. Chen, Y. Liao, G. Lv, A. Tjörnebo, F. Narjes, HTS followed by NMR based counterscreening. Discovery and optimization of pyrimidones as reversible and competitive inhibitors of xanthine oxidase, Bioorg. Med. Chem. Lett. 24 (2014) 1315-1321.

[21] S. Wang, J. Yan, J. Wang, J. Chen, T. Zhang, Y. Zhao, M. Xue, Synthesis of some 5-phenylisoxazole-3-carboxylic acid derivatives as potent xanthine oxidase inhibitors, Eur. J. Med. Chem. 45 (2010) 2663-2670.

[22] K. Nepali, A. Agarwal, S. Sapra, V. Mittal, R. Kumar, U.C. Banerjee, M.K. Gupta, N.K. Satti, O.P. Suri, K.L. Dhar, N-(1,3-Diaryl-3-oxopropyl)amides as a new template for xanthine oxidase inhibitors, Bioorg. Med. Chem. 19 (2011) 5569-5576.

[23] K. Nepali, G. Singh, A. Turan, A. Agarwal, S. Sapra, R. Kumar, U.C. Banerjee, P.K. Verma, N.K. Satti, M.K. Gupta, O.P. Suri, K.L. Dhar, A rational approach for the design and synthesis of 1-acetyl-3,5-diaryl-4,5-dihydro(1H)pyrazoles as a new class of potential non-purine xanthine oxidase inhibitors, Bioorg. Med. Chem. 19 (2011) 1950-1958.

[24] E. Hofmann, J. Webster, T. Do, R. Kline, L. Snider, Q. Hauser, G. Higginbottom, A. Campbell, L. Ma, S. Paula, Hydroxylated chalcones with dual properties: Xanthine oxidase inhibitors and radical scavengers, Bioorg. Med. Chem. 24 (2016) 578-587.

[25] R.M. Vitale, L. Antenucci, M. Gavagnin, G. Raimo, P. Amodeo, Structure-activity relationships of fraxamoside as an unusual xanthine oxidase inhibitor, J. Enzyme Inhib. Med. Chem. 32 (2017) 345-354.

[26] M. Kaur, A. Kaur, S. Mankotia, H. Singh, A. Singh, J.V. Singh, M.K. Gupta, S. Sharma, K. Nepali, P.M. Bedi, Synthesis, screening and docking of fused pyrano[3,2-d]pyrimidine derivatives as xanthine oxidase inhibitor, Eur. J. Med. Chem. 131 (2017) 14-28.

[27] T.-j. Zhang, S.-y. Li, W.-y. Yuan, Q.-x. Wu, L. Wang, S. Yang, Q. Sun, F.-h. Meng, Discovery and biological evaluation of some (1H-1,2,3-triazol-4-yl)methoxybenzaldehyde derivatives containing an anthraquinone moiety as potent xanthine oxidase inhibitors, Bioorg. Med. Chem. Lett. 27 (2017)

729-732.

[28] H.J. Tang, X.W. Zhang, L. Yang, W. Li, J.H. Li, J.X. Wang, J. Chen, Synthesis and evaluation of xanthine oxidase inhibitory and antioxidant activities of 2-arylbenzo[b]furan derivatives based on salvianolic acid C, Eur. J. Med. Chem. 124 (2016) 637-648.

[29] M.R. Ali, S. Kumar, O. Afzal, N. Shalmali, W. Ali, M. Sharma, S. Bawa, 2-Benzamido-4-methylthiazole-5-carboxylic Acid Derivatives as Potential Xanthine Oxidase Inhibitors and Free Radical Scavengers, Arch. Pharm. (Weinheim) 350 (2017) e1600313.

[30] S. Chen, T. Zhang, J. Wang, F. Wang, H. Niu, C. Wu, S. Wang, Synthesis and evaluation of 1-hydroxy/methoxy-4-methyl-2-phenyl-1H-imidazole-5-carboxylic acid derivatives as non-purine xanthine oxidase inhibitors, Eur. J. Med. Chem. 103 (2015) 343-353.

[31] A. Heidari, M.H. Fatemi, Comparative molecular field analysis (CoMFA), topomer CoMFA, and hologram QSAR studies on a series of novel HIV-1 protease inhibitors, Chem. Biol. Drug Des. 89 (2017) 918-931.

[32] K. Matsumoto, K. Okamoto, N. Ashizawa, T. Nishino, FYX-051: A Novel and Potent Hybrid-Type Inhibitor of Xanthine Oxidoreductase, J. Pharmacol. Exp. Ther. 336 (2010) 95-103.

[33] G.M. Morris, R. Huey, W. Lindstrom, M.F. Sanner, R.K. Belew, D.S. Goodsell, A.J. Olson, AutoDock4 and AutoDockTools4: Automated docking with selective receptor flexibility, J. Comput. Chem. 30 (2009) 2785-2791.

[34] D. Mandalapu, B. Kushwaha, S. Gupta, N. Singh, M. Shukla, J. Kumar, D.K. Tanpula, S.N. Sankhwar, J.P. Maikhuri, M.I. Siddiqi, J. Lal, G. Gupta, V.L. Sharma, 2-Methyl-4/5-nitroimidazole derivatives potentiated against sexually transmitted Trichomonas: Design, synthesis, biology and 3D-QSAR study, Eur. J. Med. Chem. 124 (2016) 820-839.

[35] R. Karki, K.Y. Jun, T.M. Kadayat, S. Shin, T.B. Thapa Magar, G. Bist, A. Shrestha, Y. Na, Y. Kwon, E.S. Lee, A new series of 2-phenol-4-aryl-6-chlorophenyl pyridine derivatives as dual topoisomerase I/II inhibitors: Synthesis, biological evaluation and 3D-QSAR study, Eur. J. Med. Chem. 113 (2016) 228-245.

[36] H.Y. Lim, J. Heo, H.J. Choi, C.Y. Lin, J.H. Yoon, C. Hsu, K.M. Rau, R.T. Poon, W. Yeo, J.W. Park, M.H. Tay, W.S. Hsieh, C. Kappeler, P. Rajagopalan, H. Krissel, M. Jeffers, C.J. Yen, W.Y. Tak, A phase II study of the efficacy and safety of the combination therapy of the MEK inhibitor refametinib (BAY 86-9766) plus sorafenib for Asian patients with unresectable hepatocellular carcinoma, Clin. Cancer Res. 20 (2014) 5976-5985.

1. Legends for Fig. 1, Fig. 2, Fig. 3, Fig. 4, Fig. 5, Fig. 6, Fig. 7, Scheme 1 and Scheme 2.

Fig. 1 Chemical structures of Allopurinol, Febuxostat, Topiroxostat and compounds **1-3**.

Fig. 2 Design of compounds **4a-g** and **5a-g.**

Fig. 3 The inhibition of XO by compound **4f**. Values are means ± SD, n = 3.

Fig. 4 Binding modes of Topiroxostat (**A**), **4f** (**B**) and **5f** (**C**) within the XO binding pocket.

Fig. 5 Contour maps of Topomer CoMFA. (**A**) Steric contour map depicted around S1; (**B**) electrostatic contour map depicted around S1; (**C**) steric contour map depicted around S2; (**D**) electrostatic contour map depicted around S2.

Fig. 6 The correlation chart of experimental versus predicted pIC_{50} values for the training set and test set compounds.

Fig. 7 Lineweaver-Burk plot analysis of XO inhibition by compound **4f**.

Scheme 1 Reagents and conditions: (i) Br_2, I_2, CH_2Cl_2, 5 °C, 24 h; (ii) BnBr, KI, K_2CO_3, DMF, N_2, 80 °C, 8 h; (iii) CuCN, DMF, 150 °C, 8 h; (iv) H_2, Pd/C, THF, 25 °C, 5 h; (v) RCl or RBr, KI, K_2CO_3, N_2, DMF, 80 °C, 8 h; (vi) t-BuONO, C_2H_5ONa, EtOH, 0~10 °C, 24 h; (vii) NH_4OAc, CH_3OH, reflux, 24 h.

Scheme 2 Reagents and conditions: NH_4OAc, CH_3OH, reflux, 24 h.

2. Graphics for Fig. 1, Fig. 2, Fig. 3, Fig. 4, Fig. 5, Fig.6, Fig. 7, Scheme 1 and Scheme 2

Fig. 1

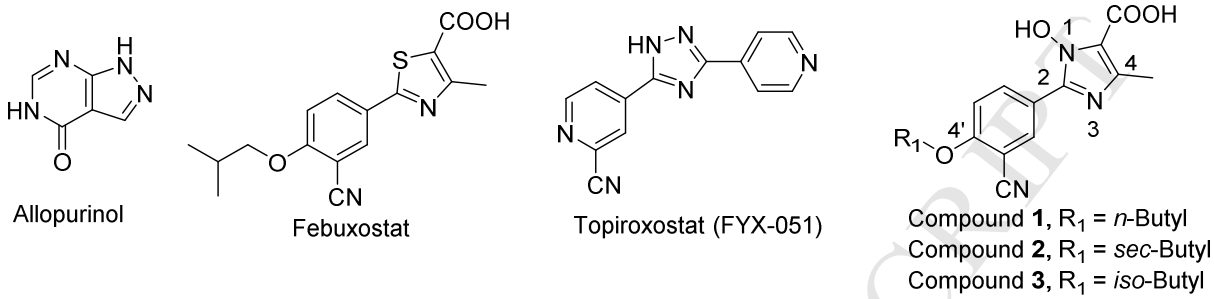

Fig. 2

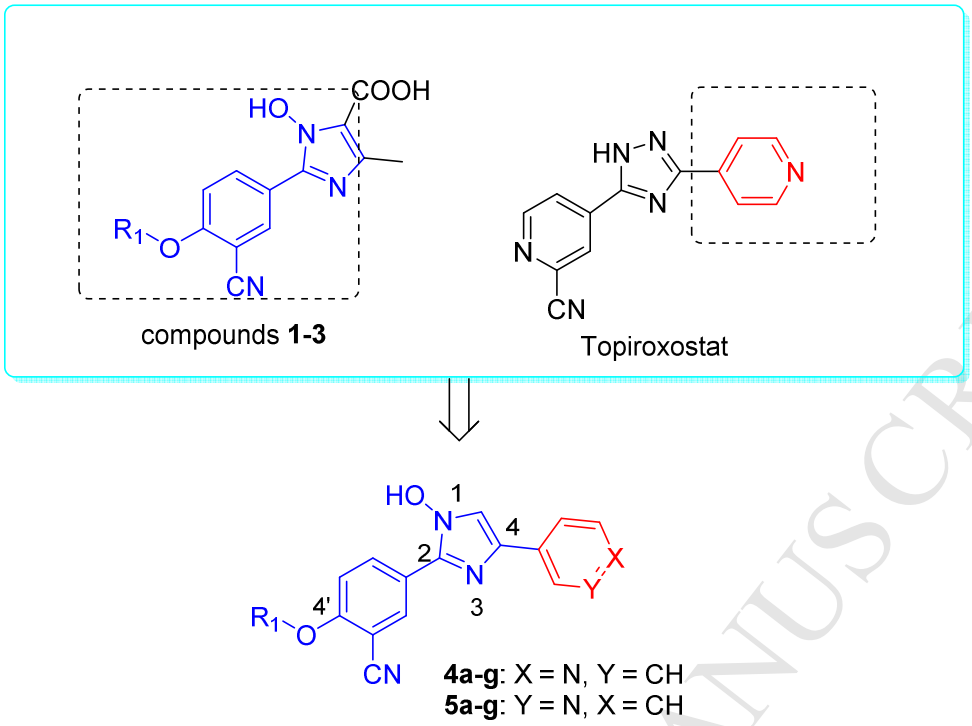

Fig. 3

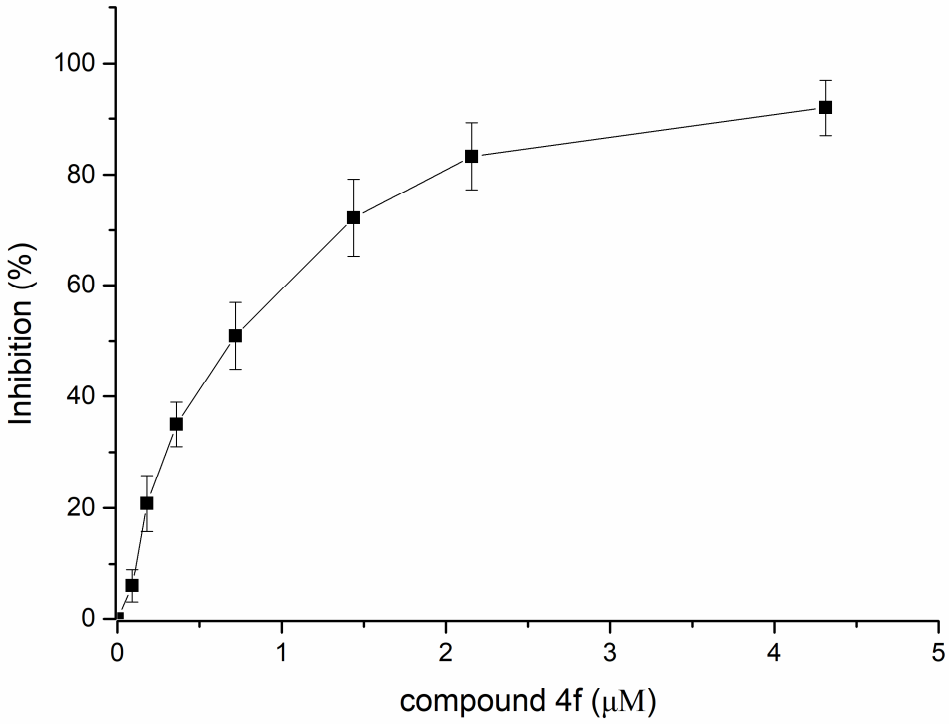

Fig. 4

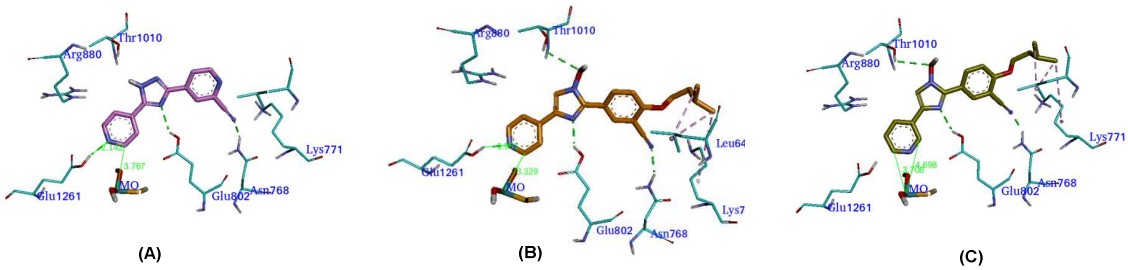

Fig 5

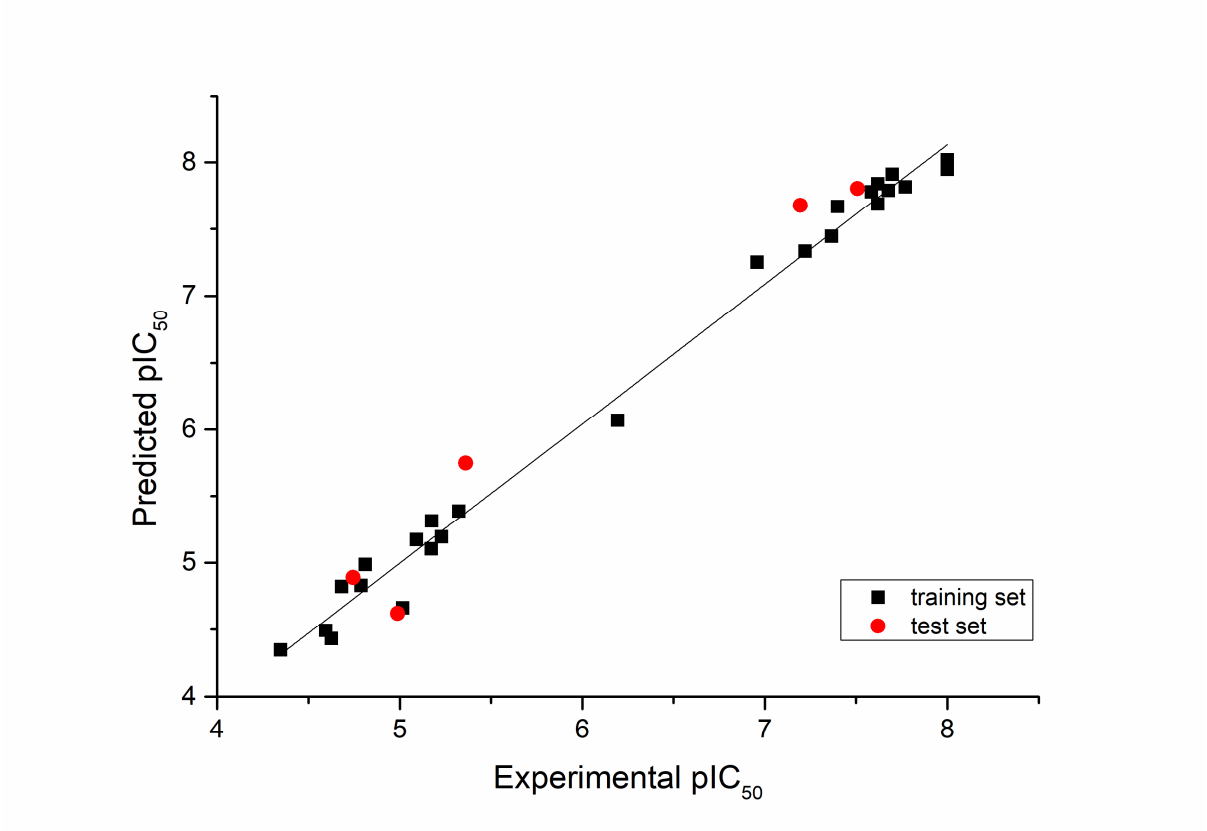

Fig. 6

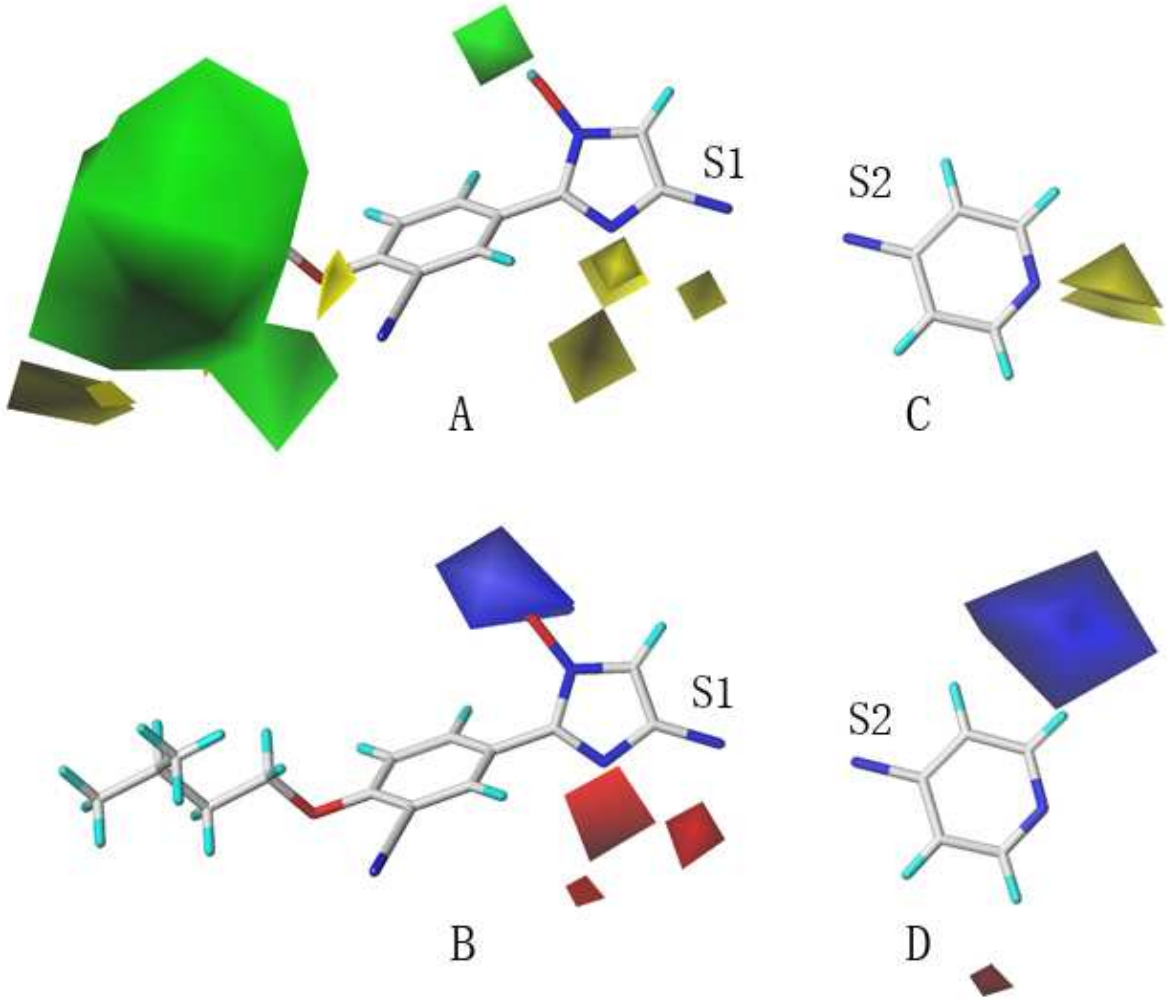

Fig. 7

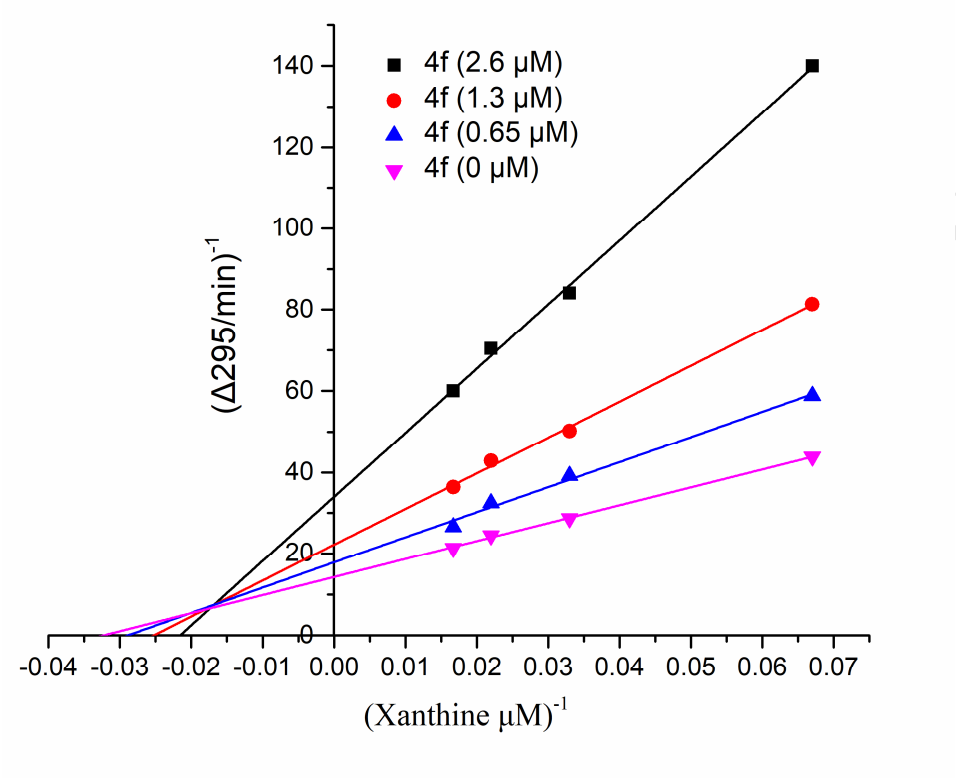

Scheme 1

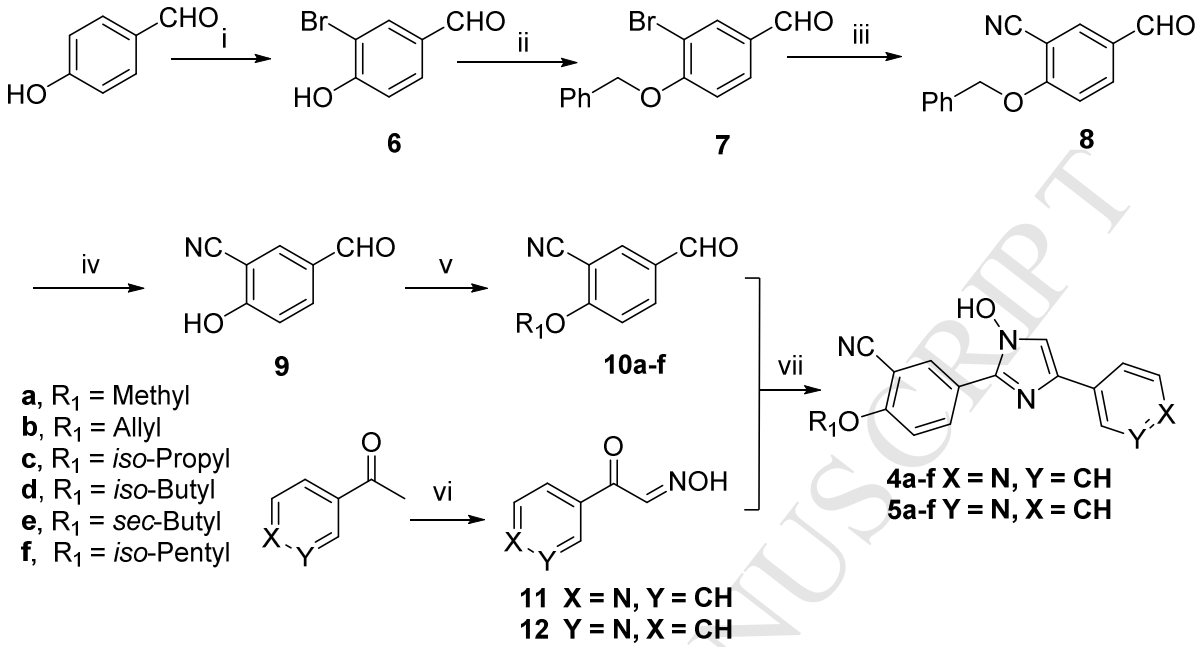

Scheme 2

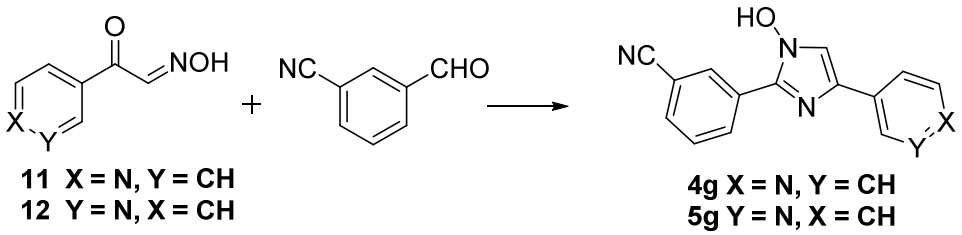

11 X = N, Y = CH
12 Y = N, X = CH

4g X = N, Y = CH
5g Y = N, X = CH

3. Table

Table.1 In vitro XO inhibitory potency of designed compounds **4a-g** and **5a-g**.

Name	R_1	IC_{50} (μM) [a]	Name	R_1	IC_{50} (μM)
4a	Methyl	15.42±0.42	**5a**	Methyl	n.a.[b]
4b	Allyl	n.a.	**5b**	Allyl	9.62±0.53
4c	*iso*-Propyl	4.75±0.19	**5c**	*iso*-Propyl	n.a.
4d	*iso*-Butyl	n.a.	**5d**	*iso*-Butyl	10.28±0.64
4e	*sec*-Butyl	4.35±0.23	**5e**	*sec*-Butyl	n.a.
4f	*iso*-Pentyl	0.64±0.04	**5f**	*iso*-Pentyl	6.73±0.42
4g	—	n.a.	**5g**	—	n.a.
Topiroxostat	—	0.0048±0.0009			

[a] Values are means±SD of three independent experiments.

[b] n.a.: not active (<50% inhibition at 10 μg/mL).

Table 2 Structures, experimental pIC_{50} and predicted pIC_{50} values of the compounds used in the Topomer CoMFA model.

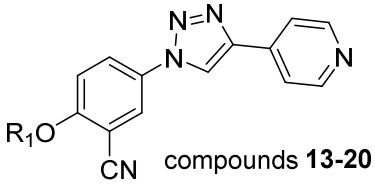

compounds **13-20**

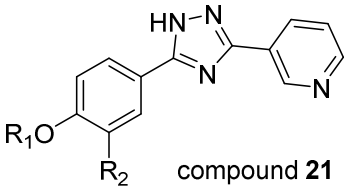

compound **21**

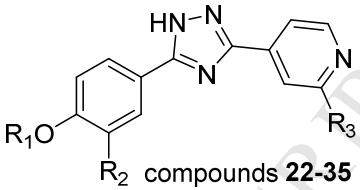

compounds **22-35**

compound	R_1	R_2	R_3	Experimental pIC_{50}	Predicted pIC_{50}	Residual	Contribution of S1	Contribution of S2
4a	Methyl	/	/	4.81	4.99	-0.18	0.64	-0.33
4c	*iso*-Propyl	/	/	5.32	5.39	-0.07	0.64	0.07
4e*	*sec*-Butyl	/	/	5.36	5.75	-0.39	0.64	0.43
4f	*iso*-Pentyl	/	/	6.19	6.07	0.12	0.64	0.75
5b	Allyl	/	/	5.02	4.66	0.36	-0.33	0.31
5d*	*iso*-Butyl	/	/	4.99	4.62	0.37	-0.33	0.27
5f	*iso*-Pentyl	/	/	5.17	5.10	0.07	-0.33	0.75

13	*n*-Butyl	/	/	4.68	4.82	-0.14	0.64	-0.49
14	*n*-Pentyl	/	/	4.79	4.83	-0.04	0.64	-0.49
15	*iso*-Propyl	/	/	4.60	4.49	0.11	0.64	-0.82
16*	*sec*-Butyl	/	/	4.74	4.89	-0.15	0.64	-0.43
17	iso-Pentyl	/	/	5.09	5.17	-0.08	0.64	-0.14
18	Cyclopentyl	/	/	5.17	5.31	-0.14	0.64	-0.01
19	Benzyl	/	/	4.35	4.35	0	0.64	-0.97
20	*para*-Methoxybenzyl	/	/	4.63	4.43	0.20	0.64	-0.88
21	*iso*-Butyl	NO_2	/	5.23	5.19	0.04	-0.33	0.84
22	*iso*-Butyl	NO_2	Methyl	8.00	8.02	-0.02	2.50	0.84
23	*iso*-Butyl	NO_2	Chloro	8.00	7.95	0.05	2.42	0.85
24	*iso*-Butyl	CN	Methyl	7.77	7.81	-0.04	2.50	0.64
25	*iso*-Butyl	COOEt	Methyl	7.70	7.91	-0.21	2.50	0.74
26	H	CN	Methyl	7.37	7.44	-0.07	2.50	0.27

27	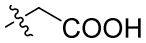	CN	Methyl	6.96	7.25	-0.29	2.50	0.08
28	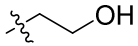	CN	Methyl	7.40	7.67	-0.27	2.50	0.49
29*	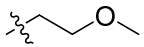	CN	Methyl	7.19	7.68	-0.49	2.50	0.50
30	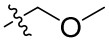	CN	Methyl	7.62	7.68	-0.06	2.50	0.51
31	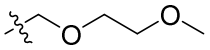	CN	Methyl	7.62	7.84	-0.22	2.50	0.66
32*	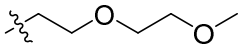	CN	Methyl	7.51	7.80	-0.29	2.50	0.63
33	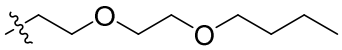	CN	Methyl	7.59	7.78	-0.19	2.50	0.60
34	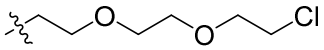	CN	Methyl	7.68	7.79	-0.11	2.50	0.61
35	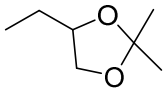	CN	Methyl	7.22	7.33	-0.11	2.50	0.16

***** Test set compounds.

4. Graphical abstract

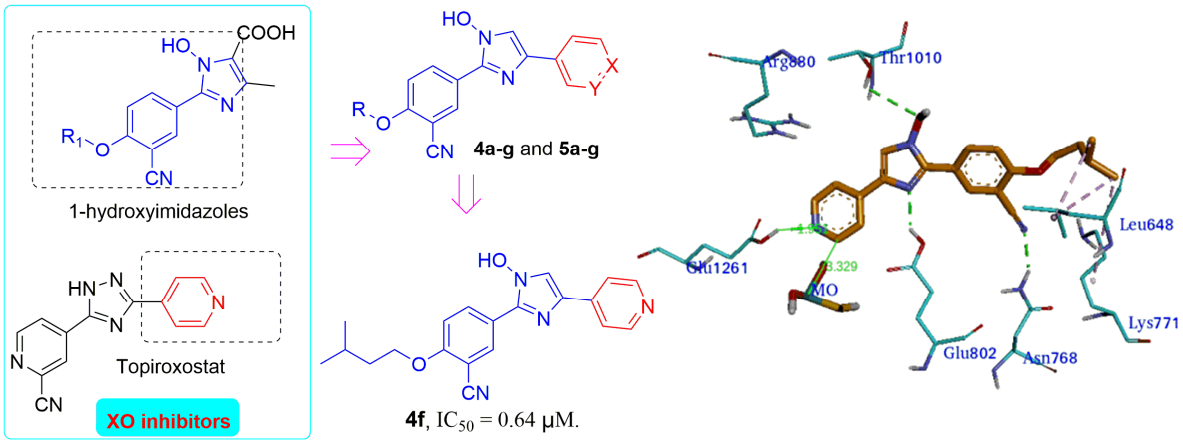

Highlights

- 1-Hydroxy-2-phenyl-4-pyridyl-1*H*-imidazole derivatives were synthesized.
- Compound **4f** showed a promising XO inhibitory potency with an IC_{50} value of 0.64 μM.
- The structure–activity relationships of the synthesized compounds were summarized.
- Molecular modeling and Steady-state kinetic analysis were performed.
- 3D-QSAR model was conducted.